J|A|C|S
ARTICLES
Published on Web 05/22/2002

Molecular-Scale Tribology of Amorphous Carbon Coatings: Effects of Film Thickness, Adhesion, and Long-Range Interactions

G. T. Gao,† Paul T. Mikulski,‡ and Judith A. Harrison*,†

Contribution from the Chemistry and Physics Departments, United States Naval Academy, Annapolis, Maryland 21402

Received December 21, 2001

Abstract: Classical molecular dynamics simulations have been conducted to investigate the atomic-scale friction and wear when hydrogen-terminated diamond (111) counterfaces are in sliding contact with diamond (111) surfaces coated with amorphous, hydrogen-free carbon films. Two films, with approximately the same ratio of sp^3-to-sp^2 carbon, but different thicknesses, have been examined. Both systems give a similar average friction in the load range examined. Above a critical load, a series of tribochemical reactions occur resulting in a significant restructuring of the film. This restructuring is analogous to the "run-in" observed in macroscopic friction experiments and reduces the friction. The contribution of adhesion between the probe (counterface) and the sample to friction was examined by varying the saturation of the counterface. Decreasing the degree of counterface saturation, by reducing the hydrogen termination, increases the friction. Finally, the contribution of long-range interactions to friction was examined by using two potential energy functions that differ only in their long-range forces to examine friction in the same system.

1. Introduction

Due to their superior tribological properties, amorphous-carbon and diamond-like carbon (DLC) films have offered tremendous opportunities in many technical applications, such as solid lubricants, protective coatings, and wear-resistant coatings.[1−5] Recently, the passivation of silicon surfaces within microelectromechanical systems (MEMS) using carbon films has been proposed to prevent stiction and to reduce friction.[6−11] A full understanding of the tribological behavior of amorphous carbon (including DLC) films is an essential issue in such applications. Therefore, amorphous carbon coatings have been the subject of intensive studies for the last 20 years.[1,5,12] A number of experiments have examined the tribology of amorphous carbon films. These experiments show that the tribological properties of amorphous carbon films are dependent upon the nature of the films, as controlled by the deposition process, and the tribotesting conditions.

Both the hydrogen content and the sp^3-to-sp^2 ratio in the films have been shown to affect the mechanical and tribological properties of DLC films.[1] In addition, experiments show that the macroscopic friction of diamond is reduced by the formation of debris, usually amorphous carbon.[13,14] Similarly, the friction of DLC films is markedly affected by tribochemical effects. The formation of a transfer film, followed by shear within the interfacial material or interfacial shear (between the transfer film and the DLC film) are the two most likely friction controlling mechanisms for DLC films.[1]

Molecular dynamics (MD) simulations have played an important role in our understanding of atomic-scale tribological processes. The atomic-scale tribological behavior between two diamond crystal surfaces has been investigated extensively using MD simulations.[15−22] Recently, we have used MD simulations

* To whom correspondence should be addressed. E-mail: jah@usna.edu.
† Chemistry Department.
‡ Physics Department.

(1) Erdemir, A.; Donnet, C. Tribology of Diamond, Diamond-Like Carbon, and Related Films. In *Modern Tribology Handbook*; CRC Press LLC: Boca Raton, FL, 2001; pp 871−908.
(2) Gruen, D. M. *Mater. Res. Soc. Bull.* **2001**, *26*, 771−776.
(3) Erdemir, A.; L., O. *J. Vac. Sci. Technol. A* **2000**, *18*, 1987−1992.
(4) Erdemir, A.; Eryilmaz, O. L.; Nilufer, I. B.; Fenske, G. R. *Diamond Relat. Mater.* **2000**, *9*, 632−637.
(5) Heimberg, J. A.; Wahl, K. J.; Singer, I. L.; Erdemir, A. *Appl. Phys. Lett.* **2001**, *78*, 2449−2451.
(6) deBoer, M. P.; Knapp, J. A.; Mayer, T. M.; Michalske, T. A. SPIE/EOS Conference on Microsystems Metrology and Inspection, 1999: http://www.mdl.sandia.gov/micromachine/docs/SPIE.0699.pdf.
(7) Dugger, M. T.; Senft, D. C.; Nelson, G. C. Friction and Durability of Chemisorbed Organic Lubricants for MEMS. In *Microstructure and Tribology of Polymer Surfaces*; Tsukruk, V. V., Wahl, K. J., Eds.; American Chemical Society: Washington, DC, 1999.
(8) Maboudian, R. *Mater. Res. Soc. Bull.* **1998**, *23*, 47−51.
(9) Mastrangelo, C. H. Surface Force Induced Failures in Microelectromechanical Systems. In *Tribology Issues and Opportunities in MEMS*; Bhushan, B., Ed.; Kluwer Academic Publishers: Norwell, MA, 1998.
(10) Tsukruk, V. V. Tribological Properties of Modified MEMS Surfaces. In *Tribology Issues and Opportunities in MEMS*; Kluwer Academic Publishers: Dordrecht, Boston, London, 1998; pp 607−614.
(11) Houston, M. R.; Howe, R. T.; Komvopoulos, K.; Maboudian, R. *Mater. Res. Soc. Sym. Proc.* **1995**, *383*, 391−402.
(12) Erdemir, A.; Fenski, G. R.; Krauss, A. R.; Gruen, D. M.; McCauley, T.; Csencsits, R. T. *Surf. Coat. Technol.* **1999**, *120−121*, 565−572.
(13) Hayward, I. P.; Singer, I. L.; Seitzman, L. E. *Wear* **1992**, *157*, 215−227.
(14) Hayward, I. P. *Surf. Coat. Technol.* **1991**, *49*, 554−559.
(15) Perry, M. D.; Harrison, J. A. *J. Phys. Chem. B* **1997**, *101*, 1364−1373.
(16) Perry, M. D.; Harrison, J. A. *Thin Solid Films* **1996**, *290−291*, 211−215.
(17) Perry, M. D.; Harrison, J. A. *J. Phys. Chem.* **1995**, *99*, 9960−9965.
(18) Perry, M. D.; Harrison, J. A. *Langmuir* **1995**, *12*, 19.
(19) Perry, M. D.; Harrison, J. A. *Tribol. Lett.* **1995**, *1*, 109−119.
(20) Harrison, J. A.; Brenner, D. W. *J. Am. Chem. Soc.* **1994**, *116*, 10399−10402.
(21) Harrison, J. A.; Colton, R. J.; White, C. T.; Brenner, D. W. *Wear* **1993**, *168*, 127−133.
(22) Harrison, J. A.; White, C. T.; Colton, R. J.; Brenner, D. W. *Phys. Rev. B* **1992**, *46*, 9700−9708.

10.1021/ja0178618

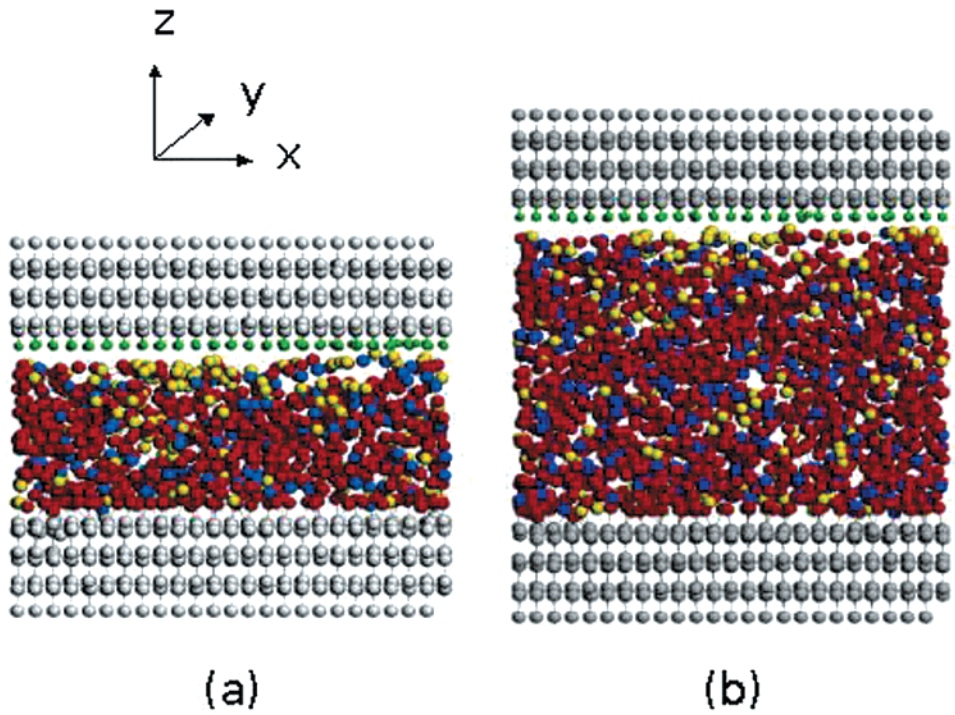

Figure 1. The thin- (a) and thick-film (b) systems. The density of the thin- and thick-film systems is 1.75 and 2.15 g/cm^3, respectively. Sliding is along the *x* direction, and indention corresponds to motion in the $-z$ direction. Carbon (large spheres) and hydrogen (small spheres) atoms in the diamond substrates are colored gray and green, respectively. Blue, red, and yellow carbon atoms in the films have sp^3, sp^2, and sp hybridization, respectively.

to examine the indentation and friction of self-assembled monolayers (SAMS) composed of *n*-alkane chains of various lengths[23] and packing densities.[24] To our knowledge, MD simulations that examine the atomic tribology of the amorphous carbon films have not been reported. In this work, we examine the atomic-scale tribological behavior of amorphous carbon films by using MD simulations. In particular, we find that the average friction versus average load curves of the carbon-film systems show a linear behavior. We also find that sliding on the carbon films at high loads can wear away hydrogen atoms from the counterface leading to a series of tribochemical reactions, between the probe and the film, and adhesion between the counterface and the film. The contribution of adhesion to friction is examined by performing several sets of simulations with different amounts of unsaturated (or radical-containing) carbon atoms on the counterface. Finally, we examine the effect of long-range interactions on the friction of amorphous films by using two potential energy functions that differ only in their long-range contributions to conduct identical sliding simulations.

2. Methods and Procedures

The simulation systems consist of hydrogen-terminated diamond (111) counterfaces brought into sliding contact with amorphous carbon films attached to the (111) face of diamond (Figure 1). The carbon films are created by heating a piece of diamond to 6000 K for 40 ps and then rapidly cooling it to 300 K while it is in contact with a diamond substrate. Two, hydrogen-free films, with 1000 (thin-film system) and 2000 carbon atoms (thick-film system), are examined. The thicknesses of the thin- and thick-film systems are 14.6 and 23.5 Å, respectively. The percentage of sp^3, sp^2, and sp hybridized carbon obtained from an analysis of the coordination number of each carbon atom in the thin-film system is 14.6%, 72.1%, and 13.3%, respectively. The thick-film system contains 15.0% (sp^3), 75.0% (sp^2), and 10.0% (sp) hybridized carbon. Thus, the sp^3-to-sp^2 ratio in both films is approximately 1:5. Because the two films are prepared in the same way, they possess similar surface structures. This was confirmed by visual analysis and calculation of the density profiles within the films.

Both the diamond substrate and the diamond counterface contain 7 layers of carbon atoms with 144 atoms per layer. The diamond counterface is terminated with hydrogen atoms to satisfy the valence requirements of carbon. Periodic boundary conditions are applied in the plane parallel to the sliding interface. The dimensions of the computation cell in the sliding plane are approximately 30.2 Å by 26.1 Å, which corresponds to 12 unit cells of diamond (111) in the sliding direction and 6 unit cells transverse to the sliding direction. The bottom layer of the diamond substrate and the top layer of the counterface are held rigid (Figure 1). Moving inward toward the carbon film, the next two layers of the substrate and the counterface are maintained at a constant temperature (300 K) by using independent Langevin thermostats.[25,26] All remaining atoms are free to move according to classical dynamics. The equations of motion for all nonrigid atoms are integrated by using the velocity Verlet algorithm with a constant step size of 0.25 fs.[27]

Unless otherwise noted, the force on each atom is described by an updated version of Brenner's reactive empirical bond-order (REBO) potential.[28,29] The parameters and the functional form of this updated REBO were altered slightly so that the potential more accurately reproduces the elastic constants of diamond and graphite while not disrupting the properties that were fit in the earlier version of the potential.[30,31] The many-body nature of the REBO potential allows the

(23) Tutein, A. B.; Stuart, S. J.; Harrison, J. A. *Langmuir* **2000**, *16*, 291−296.
(24) Mikulski, P. T.; Harrison, J. A. *J. Am. Chem. Soc.* **2001**, *123*, 6873−6881.
(25) Swope, W. C.; Andersen, H. C.; Berens, P. H.; Wilson, K. R. *J. Chem. Phys.* **1982**, *76*, 637−649.
(26) Adelman, S. A.; Doll, J. D. *J. Chem. Phys.* **1976**, *64*, 2375−2388.
(27) Verlet, L. *Phys. Rev. B* **1967**, *159*, 98.
(28) Brenner, D. W. *Phys. Stat. Solid b* **2000**, *217*, 23.
(29) Brenner, D. W.; Shenderova, O. A.; Harrison, J. A.; Stuart, S. J.; Ni, B.; Sinnott, S. B. *J. Phys. Condens. Matter* **2002**, *14*, 783−802.
(30) Brenner, D. W. *Phys. Rev. B* **1990**, *42*, 9458−9471.
(31) Brenner, D. W.; Harrison, J. A.; Colton, R. J.; White, C. T. *Thin Solid Films* **1991**, *206*, 220−223.

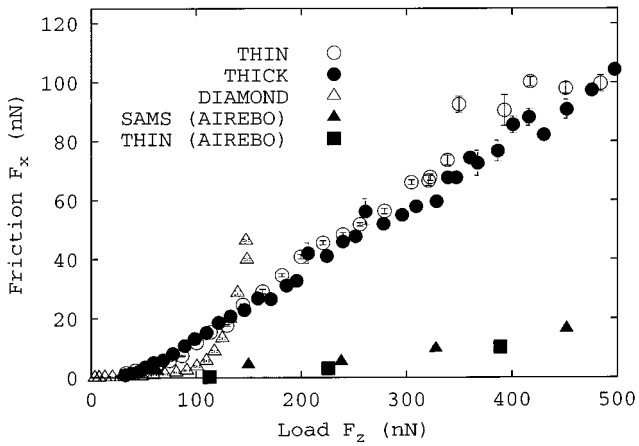

Figure 2. Friction curves for the thin-film system (open circles), for the thick-film system (filled circles), for hydrogen-terminated diamond (open triangles), a monolayer of C_{18} alkane chains (filled triangles) calculated with the AIREBO potential, and the thin-film system (filled squares) calculated with the AIREBO potential (filled squares). Error bars represent one standard deviation and their calculation is discussed in the text.

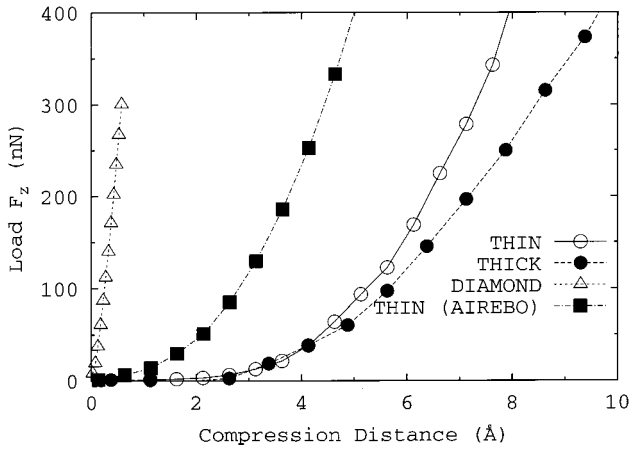

Figure 3. Compression curves for the thin-film system, thick-film system, diamond on diamond, and the thin-film system calculated with the AIREBO potential. Compression distance is defined in the text. Symbols are the same as in Figure 2. Error bars that are not visible are smaller than the squares.

bond energy of each atom to depend on its local environment. Therefore, this is one of the few empirical potentials that allows for chemical reactions and the accompanying changes in atomic hybridization. As a result, wear events can be simulated.[20,32] Intermolecular forces were added to the REBO potential by using a novel adaptive algorithm to maintain the reactive nature of the potential energy function.[33] This adaptive intermolecular REBO (AIREBO) potential has been used here to elucidate the effect of long-range interactions on friction. Compression of the carbon films is accomplished by moving the rigid layer of the countersurface at a constant velocity of 10 m/s toward the carbon film. Sliding of the countersurface is performed by moving the same layers at a constant velocity of 100 m/s in the sliding direction (left to right in Figure 1) while maintaining a constant separation between the rigid layers. The load and friction forces are taken to be the forces on the atoms in the rigid layer perpendicular to the plane that contains the film and parallel to the sliding direction, respectively.

3. Results and Discussion

3.1. Friction Curves. Friction force as a function of load is shown in Figure 2 for both the thick- and thin-film systems. To eliminate the influence of startup effects that arise from the abrupt transition from compression to sliding, data from the first 15 ps of sliding are ignored. The remainder of the slide is partitioned into 6 unit-cell bins. The instantaneous friction in each unit-cell bin is averaged and each point in Figure 2 corresponds to the average of these 6 unit-cell bins. The error bars represent the standard deviation of the average friction from the 6 unit-cell bins during a given slide. For comparison, friction versus load data for several other systems are included in Figure 2. These systems have a hydrogen-terminated diamond counterface in sliding contact with a hydrogen-terminated diamond (111) surface, the thin-film system (friction calculated with the AIREBO potential), and a tightly packed monolayer of C_{18} alkane chains[24] (friction calculated with the AIREBO potential).

For the simulations performed with the REBO potential, the calculated friction of the thick- and thin-film systems increases linearly with load and is independent of film thickness. Below approximately 130 nN, the friction of the diamond−diamond system is lower than that of the film-containing systems. At higher loads, the friction of the diamond−diamond system increases markedly with load and is much larger than the film-containing systems. Friction for the two systems calculated with the AIREBO potential (the C_{18} monolayer and the thin-film system) is a linear function of load but is significantly smaller than the friction calculated with the REBO potential.

Scanning probe microscope experiments have examined the connection between friction and surface order[34] and friction and elastic modulus of the substrate.[35] Meyer et al.[35] examined the friction of Langmiur−Blodgett films composed of hydrocarbon and fluorocarbon domains. The differences in the measured friction in the different domains was attributed to differences in the elastic modulus in those regions. Softer domains allowed for increased contact area between the tip and the substrate and thus an increased pull-off force (or adhesion) at a given load. As a result, the measured friction is higher. The load on the counterface versus distance moved, i.e., compression curves, is plotted in Figure 3. Each point shown in Figure 3 is averaged over a 2.5 ps interval to obtain a smooth curve. The compression distance is defined as the distance between the two surfaces, with the zero point defined as the point when the load on the upper surface becomes larger than zero. Because the slope of the compression curve at each point is proportional to the elastic modulus of the surface[36] and the same type of counterface was used in all the compressions, the greater the slope of the lines in Figure 4 the greater the stiffness of the material. Thus, the uncoated diamond surface is the stiffest material examined and the compression-curve data are linear throughout the entire load range examined. Regardless of the potential energy function used, the compression curves for the other systems in Figure 4 have two distinct slopes. The smaller slope during the initial stages of compression is largely due to the response of the films (or the alkane monolayer) to the applied load. The change in slope upon continued compression is likely due to the influence of the underlying diamond substrate. The effect of the underlying

(32) Harrison, J. A.; Stuart, S. J.; Perry, M. D. The Tribology of Hydrocarbon Surfaces Investigated using Molecular Dynamics. In *Tribology Issues and Opportunities in MEMS*; Kluwer Academic Publishers: Dordrecht, Boston, London, 1998; pp 285−299.
(33) Stuart, S. J.; Tutein, A. B.; Harrison, J. A. *J. Chem. Phys.* **2000**, *112*, 6472−6486.
(34) Lee, S.; Shon, Y.-S.; Colorado, R.; Guenard, R. L.; Lee, T. R.; Perry, S. S. *Langmuir* **2000**, *16*, 2220−2224.
(35) Overney, R. M.; Meyer, E.; Frommer, J.; Guntherodt, H.-J. *Langmuir* **1994**, *10*, 1281−1286.
(36) Pharr, G. M.; Oliver, W. C.; Brotzen, F. R. *J. Mater. Res.* **1992**, *7*, 613−617.

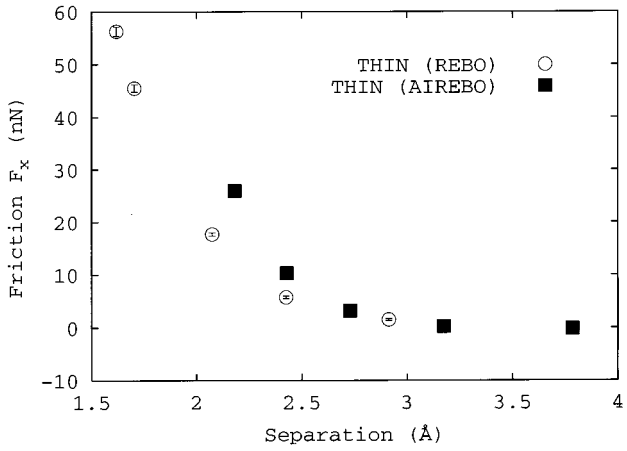

Figure 4. Friction as a function of separation between the counterface and the surface of the thin film for simulations conducted with the AIREBO and the REBO potentials. Error bars represent one standard deviation. Symbols are the same as Figures 2 and 3.

substrate is also evident if one compares the thick- and thin-film simulations performed with the REBO potential. The slope of the compression curves is very similar for small compressions. The thin-film system "feels" the presence of the diamond substrate after a smaller degree of compression. Thus, the two curves diverge. After this point, the thin-film system has a larger slope because the diamond substrate is harder than the film.

Comparison of the compression curves for the thin-film simulations that utilize the REBO and the AIREBO potentials demonstrates that the presence of long-range forces has little influence the slope of the curve. Because the slope of the curve is largely due to the short-range interactions within the film, and these are the same in both potentials, this result is not surprising. The long-range forces present in the AIREBO potential cause the forces in the compression curve to become nonzero at smaller values distances because the potential acts over longer distances. In other words, because the same starting configuration was used in both thin-film simulations, the load on the counterface becomes nonzero at larger separations (smaller distance moved) when the AIREBO potential is used.

For the simulations conducted with the REBO potential, the material with the larger Young's Modulus has lower friction (for small loads) in agreement with data obtained from SPM experiments.[35] However, this agreement with experiment at small loads does not originate from differences in contact area between samples. The periodic boundary conditions employed in these simulations cause the probe (counterface) to be infinite in extent, that is, it has no edges. As a result, no penetration of the monolayer is possible. Thus, the contact area is the same in all the systems examined at all loads and it does not vary depending upon the elastic modulus of the material as it might in an SPM experiment.

It should also be noted that simulation conditions, such as sliding speed and temperature, are identical in the results presented here except for the potential energy function. As indicated earlier, a reparametrized version of Brenner's REBO[28,29] potential was used for some of the simulations discussed here. Comparison of the friction versus load data for the thin-film system by using the REBO and AIREBO potentials (Figure 2) reveals that the AIREBO potential yields lower friction at a given load. The AIREBO potential is identical with the REBO potential except that long-range interactions and torsional interactions about single bonds have been added. Simulations have also been conducted with the AIREBO potential with the additional torsional contributions "turned off". These sliding simulations yield the identical friction with load behavior shown in Figure 2 for the simulations with use of the full AIREBO potential. Thus, it is the long-range interactions, or the Lennard-Jones portion of the potential, that give rise to the differences in friction with load for the two thin-film systems shown in Figure 2. If one considers the thin-film system with a fixed separation between the counterface and the top of the film, the long-range forces present in the AIREBO potential cause the load to be much higher than it would be in the absence of these forces. In other words, for a given load the counterface is farther from the thin film when the AIREBO potential is used, thus the friction is lower. A plot of friction versus separation between the counterface and the thin-film (Figure 4) shows that the two potentials actually yield similar values of friction at a given separation distance.

A number of SPM experiments have examined the connection between friction and order. Perry and co-workers[34] used surface science techniques and the AFM to unambiguously show that more ordered (more tightly packed) SAMS have lower friction than disordered SAMS (lower packing density). Molecular dynamics simulations have also been used to investigate friction as a function of packing density.[24] These simulations showed that a more loosely packed (disordered) C_{18} monolayer has a slightly higher friction than a tightly packed monolayer at moderate and high loads in qualitative agreement with data obtained with the AFM. The thin- and thick-film systems examined here have a similar structure at the interface and thus have similar levels of disorder.

At loads below approximately 120 nN (Figure 2), which are likely to be in the load range probed by AFM experiments, diamond has lower friction than the disordered thin- and thick-film systems. The sharp increase in friction at higher loads for the uncoated diamond surface is due to several factors. Because the uncoated diamond surface has a large elastic modulus compared to the thin film, it is fairly incompressible. Thus, over the load range examined the uncoated diamond surface is compressed approximately 0.10 Å while the thin film on the diamond is compressed about 0.8 Å. For a given load, the uncoated diamond surface is much closer to the probe surface than the thin film (Figure 5). Moreover, the hydrogen atoms on the probe and the uncoated diamond surface are aligned in the sliding direction. Previous MD simulations on this system have shown when the probe and the surface are in this geometry the opposing hydrogen atoms interact in a "head-on" manner resulting in an increase in the friction force during sliding.[22] (The results presented in this early MD work were recently confirmed using *ab initio* calculations.[37]) For the hydrogen atoms on the probe to "pass by" the hydrogen atoms on the diamond surface, these atoms must "revolve" around each other. This type of "head-on" interaction, coupled with the close proximity of the probe to the uncoated diamond, is responsible for the sharp increase in friction values at high loads.

Previous MD simulations that examined the friction in tightly and loosely packed C_{18} monolayers demonstrated that the calculated friction on the counterface was tightly correlated with

(37) Neitola, R.; Pakkanen, T. A. *J. Phys. Chem. B* **2001**, *105*, 1338−1343.

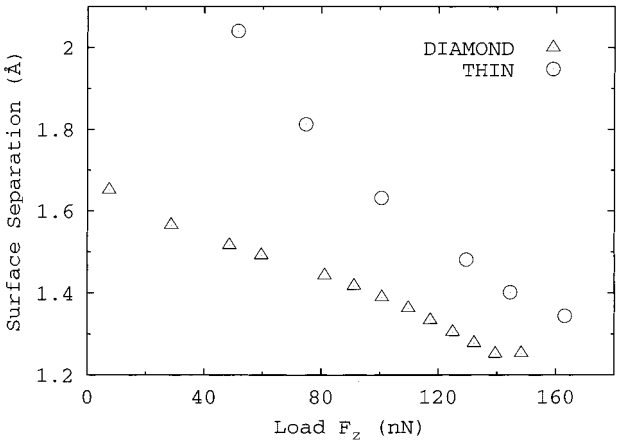

Figure 5. Surface separation between the counterface and the diamond and thin-film system as a function of load. Symbols are the same as Figure 2.

bond-length fluctuations in the carbon−carbon bonds of the alkane monolayers.[24] While the correlation is less striking here, this is also the case for the amorphous carbon films examined in this work. The time-correlation function between the average bond length in the upper, middle, and lower one-third of the film and the friction was calculated. It is clear from these data that the bond length in all portions of the thin film is correlated with the friction with the strongest correlation between the upper one-third of the film and the friction.

3.2. Wear and Friction. Experiments that have examined the friction of DLC and diamond have shown that chemical reactions induced by sliding significantly impact friction.[1,3,12−14,38,39] For example, Hayward and Singer showed that friction is reduced by the formation of amorphous carbon debris when diamond slides against diamond. Because tribochemical reactions alter the nature of the contacting interface, the friction is altered. Previous MD simulations have examined the effects of debris present prior to, and debris formed during, sliding on friction when diamond is in sliding contact with diamond. These simulations showed that small hydrocarbon-debris molecules present prior to sliding significantly reduce the friction between contacting diamond surfaces[15,16,18,19] and, under certain conditions, can initiate tribochemical reactions. In addition, molecules that are chemisorbed to diamond (111) surfaces in sliding contact can be worn from the surfaces creating debris at the interface that is consistent with the debris observed in macroscopic friction experiments.[13,14,20,32,40,41]

Tribochemistry can also occur when a diamond counterface is in sliding contact with an amorphous carbon film. A tribochemical reaction that depicts wear of the diamond counterface is shown in Figure 6. The series of reactions that is depicted in Figure 6 is initiated by the rupture of a carbon−hydrogen bond in the diamond counterface that occurs after 13.2 Å of sliding. Once this bond has been ruptured, the free hydrogen atom bonds with the carbon film. Continued sliding leads to the formation of a chemical bond between an sp^2 carbon atom in the film and the radical-containing carbon atom in the counterface. In other words, there is a "bridge" of bonded atoms that connects the counterface and the film. This small connection between the film and the counterface is shortlived, however. The counterface carbon atom with the nascent bond is transferred from the counterface by further sliding and incorporated into the film. Additional wearing of the diamond probe occurs if other unsaturated carbon atoms form bonds with film atoms. It should be noted that no wear of the counterface was observed in the 30 ps simulations with loads lower than 300 nN. In addition, in the simulation depicted in Figure 6 a number of chemical reactions occur within the film prior to the wearing of the counterface (described below).

The instantaneous friction force as a function of sliding distance for the simulation described above has several interesting features (Figure 7): the oscillatory nature of these data during the entire slide and the marked drop in the average friction during the last half of the simulation. These features can be elucidated from a detailed analysis of the bonding network within the carbon film and how this network changes during sliding.

Carbon atoms within the film are vibrating. The characterization of these vibrations can aid in the representation of the evolving bond network. Analysis of the bond lengths within the film during the course of the sliding reveals that two carbon atoms are bound when their minimum bond length oscillates below R_{min} (taken to be 1.6 Å) and their maximum bond length oscillates below R_{max} (taken to be 1.9 Å). There is a subset of carbon-atom pairs that adheres to this criterion for the duration of the simulation. That is, they remain intact or bound during the entire 120 Å of sliding. The remaining carbon-atom pairs do not adhere to this criterion for the duration of the slide. Thus, they take part in tribochemical reactions.

First, a detailed examination of the carbon-atom pairs that remain intact was undertaken. For the purpose of this analysis, the distance between the carbon-atom pairs was treated as a vector. This allows the bonds to be separated into two categories: those tilted, or with components parallel to the sliding direction and those against the sliding direction. The number of carbon-atom pairs tilted along the sliding direction as a function of sliding distance is shown in Figure 7. There are 1429 carbon-atom pairs (bonds) that remain intact during the course of the simulation. Prior to the start of sliding, approximately half of the bonds are oriented along the sliding direction and half are against the sliding direction. There is a rapid rise in the number of bonds oriented along the sliding direction as sliding is initiated (in the first angstrom of sliding). In this region, the film is "adjusting" to the sliding motion of the counterface. Bonds that were close to perpendicular to the plane of the film, but oriented against the sliding direction, are pushed into alignment with the sliding direction.

During the next 50 Å of sliding, the number of bonds oriented along the sliding direction oscillates and the average number of bonds increases from approximately 790 to 810. The oscillatory behavior is due to the hydrogen atoms from the diamond counterface interacting with the atoms in the film. The hydrogen atoms "push" on the carbon atoms in the film causing them to be aligned with the sliding direction. When the hydrogen atoms move away from a given carbon atom it "springs" back to a position that may not be oriented with the sliding direction. This interpretation is supported by the fact that the period of the oscillation matches the spacing between the hydrogen atoms

(38) Yen, B. K. *Wear* **1996**, *192*, 208.
(39) Bowden, F. P.; Young, J. E. *Proc. R. Soc. London A* **1951**, *208*, 444.
(40) Feng, Z.; Field, J. E. *Surf. Coat. Technol.* **1991**, *47*, 631−645.
(41) Wilks, J.; Wilks, E. M. *The Properties of Diamond*; Academic Press: London, 1979.

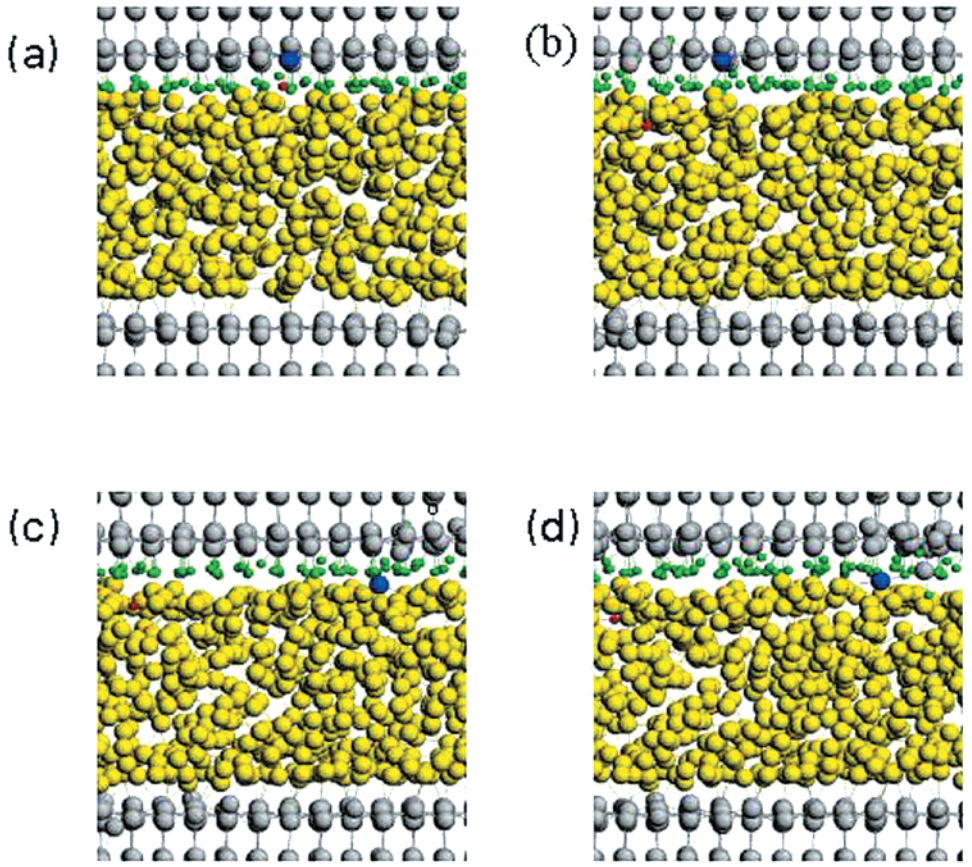

Figure 6. A series of chemical reactions induced by sliding of the counterface over the thin film under an average load of 300 nN. (a) The sliding causes the rupture of a carbon−hydrogen bond (blue and red) in the counterface. (b) The hydrogen atom (red) is incorporated into the film and forms a bond to a carbon atom in the film. (c) A bond is formed between the unsaturated carbon atoms in the film and the carbon that suffered the bond rupture in the counterface, and continued sliding causes this carbon being transferred into the film. (d) The transferred carbon forms a bond with another carbon in the counterface. The counterface has slid 0.0 (a), 15.9 (b), 26.1 (c), and 30.5 Å (d).

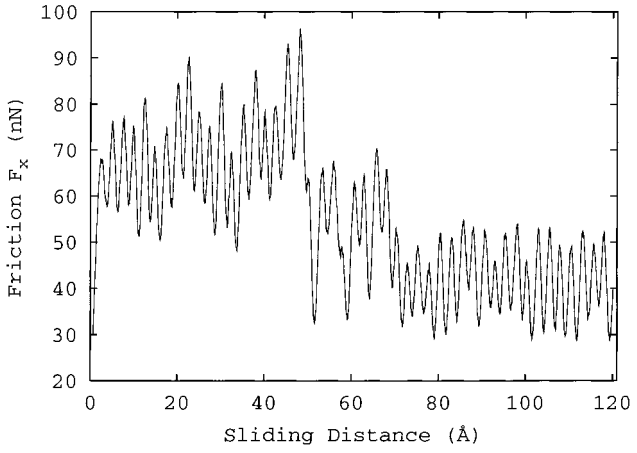

Figure 7. Friction versus sliding distance for the thin-film system calculated with the REBO potential. To smooth the curve, data shown in the figure are the averaged over 5 ps intervals. The average load during the slide is 300 nN.

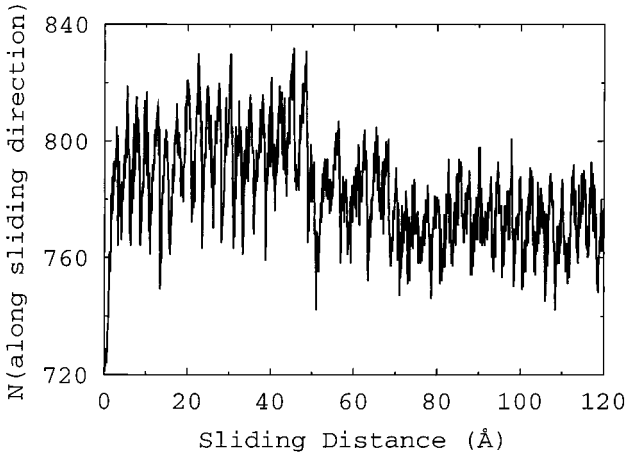

Figure 8. Number of carbon−carbon bonds within the film oriented in the sliding direction versus sliding distance.

on the counterface. The general increase in the number of bonds oriented along the sliding direction increases due to a general restructuring of the film caused by the sliding. Between 60 and 80 Å, there is a general decrease in the number of bonds oriented in the sliding direction. After 80 Å, the average number of bond oriented in the sliding direction levels out at approximately 770 bonds. Comparison of Figures 7 and 8 reveals that the shapes of these curves are very similar.

It is clear from Figure 8 that there is a marked restructuring of the film between 50 and 80 Å. In an effort to quantify this restructuring, the subset of bonds that do not remain intact during sliding were examined. A new atom pair is added to the bond set once the interatomic distance drops below R_{min}. When the interatomic distance of a carbon-atom pair from the bond set exceeds R_{max}, the pair is removed from the set. Thus, this characterization of vibration eliminates the noise associated with using a single cutoff to specify the formation and breaking of bonds.

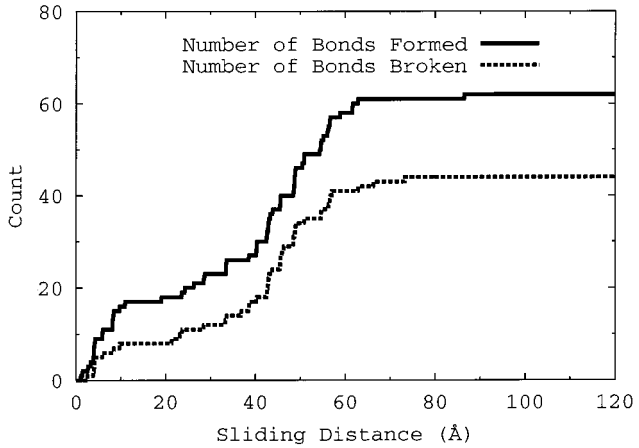

Figure 9. Number of carbon−carbon bonds formed (solid line) and broken (dashed line) within the film as a function of sliding distance. The difference between the two is the net increase in the number of bonds.

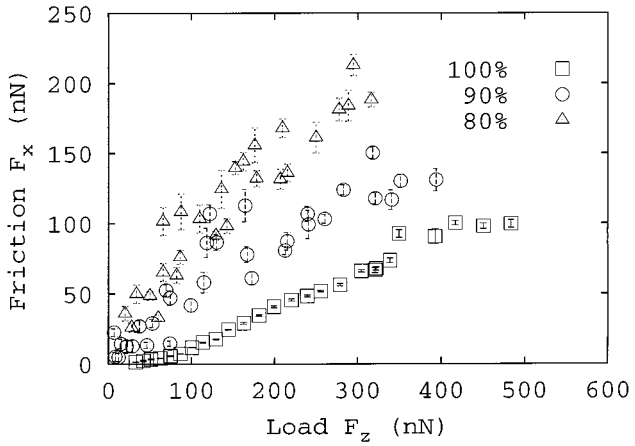

Figure 10. Friction curves for the thin-film system with a counterface that is fully or 100% hydrogen terminated (open squares), 90% hydrogen terminated (filled squares), and 80% hydrogen terminated (open circles).

The formation and breaking of bonds as a function of sliding time is shown in Figure 9. At the beginning of the slide, the number of bonds formed and broken increases gradually and then levels out. Between approximately 40 and 65 Å, both quantities increase dramatically. This coincides with the marked restructuring of the film indicated in Figure 7. After approximately 65 Å of sliding, the bond network stabilizes. Thus, the film has achieved a steady-state structure. This structure results in a lower average friction than the structure of the film present during the first half of the sliding (Figure 7). Thus, tribochemical reactions have substantially changed the nature of the interface and the calculated friction.

It should be noted that the majority of the tribochemical reactions occur within the film and not between the counterface and the film. Figure 9 clearly shows that tribochemistry occurs almost immediately within the film while the counterface slides for 13.2 Å before the initiation of reactions between the counterface in 30 ps of sliding and the film. A critical load of 300 nN or above must be achieved to observe wear of the counterface. In contrast, chemical reactions occur within the film at loads lower than 300 nN. It should also be noted that the restructuring of the film occurs as a result of the larger number of intrafilm reactions and a smaller number of reactions between the probe and the film. Thus, it appears that both types of reactions are linked to the restructuring of the film.

3.3. Adhesion and Friction. Recent experimental studies have shown that the friction coefficient increases rapidly when adsorbed gases are removed with use of thermal desorption[1] from diamond surfaces in sliding contact. This suggests that unsaturated or radical-containing surface atoms, which were passivated by these gases, are no longer passivated. Thus, they can form strong adhesive bonds with the atoms on the contacting surface. Conversely, if a clean surface of diamond is exposed to gaseous contaminants, the friction coefficient drops rapidly. This is presumably due to the passivation of the unsaturated surface atoms.

Simulations discussed here have shown that when a hydrogen atom is worn from the counterface, the carbon atom originally bonded to it forms an adhesive bond with an unsaturated carbon atom in the amorphous film. Therefore, it is conceivable that a counterface without full passivation of the carbon atoms with hydrogen can cause the friction to increase compared with a counterface with full hydrogen termination. To test this hypothesis, simulations were performed with the thin-film system using the REBO potential and several partially hydrogen-terminated diamond counterfaces.

Two additional counterfaces were examined in this part of study: one with 90% of the carbon atoms on the counterface hydrogen terminated and one with 80% termination. The hydrogen atoms that were removed were chosen randomly and all other simulation conditions remain the same. The average friction as a function of average load for the fully terminated counterface and the two partially terminated counterfaces is shown in Figure 10. In general, the two partially terminated counterfaces yield much larger friction values at a given load than the fully terminated counterface. This indicates that adhesion due to the bonding between a carbon on the counterface and a carbon in the film contributes significantly to the friction. It is also worth noting decreasing the level of hydrogen termination on the counterface causes tribochemical reactions (adhesion and wear) to occur at much lower loads than when the fully terminated counterface was used. This is apparent in the "spread" of these data in Figure 10. For example, when the counterface is 80% terminated, there is a wide range of loads that yield approximately the same value of friction (100 nN).

4. Summary

In this work, MD simulations have been used to examine the atomic-scale friction and wear when diamond (111) surfaces are in sliding contact with amorphous carbon films on diamond substrates. These simulations explored the effects of film thickness, counterface termination, and long-range interactions on tribological properties. Detailed tribochemical reactions were identified and their effect on friction and wear discussed.

The simulation results presented here suggest that the structure of the film, especially the sp^3-to-sp^2 ratio, can have a profound influence on the tribological properties of the film. These simulations clearly show that triochemical reactions can lead to adhesion between the counterface and the films and a restructuring of the film due to reactions within the film. Adhesion between the probe and the film increases the calculated friction while tribochemical reactions within the film led to a restructuring of the film and a reduction in friction. The tribochemical reactions observed here involve sp^2 carbon

atoms in the film. Thus, it is likely that films that contain a larger fraction of surface sp^2-hybridized carbon will exhibit higher levels of friction than those films with more surface sp^3-hybridized carbon. This increase in friction would likely be due to the increased adhesion from tribochemistry. It should also be noted that changing the sp^3-to-sp^2 ratio within a carbon film will also change its hardness and may also change the film's phonon frequencies. Increasing the hardness of the film may also decrease the contact area between the probe and the sample in an experimental situation. Changing the contact area can also affect the measured friction. In the results presented here, the contact area is constant. Therefore, any change in adhesion is purely due to tribochemical reactions between the probe and the film. Friction also arises from the dissipation of energy via phonon modes. The simulations presented here have not attempted to examine the changes in phonon frequencies with the films as a function of sp^3-to-sp^2 ratio. This will be the subject of future simulations.

Erdemir et al. have examined the friction of microcrystalline diamond (MCD) and nanocrystalline diamond (NCD).[12] The NCD films exhibit a period of high friction, or "run-in", when rubbing starts. Continued rubbing leads to wear and reduces the friction. An analogous situation is observed in the simulations presented here (Figures 6−9). In addition, recent AFM experiments suggest "run-in" occurs at the nanoscale.[42] During the initial stages of sliding the average friction rose gradually as the structure of the film changed. A dramatic decrease in the friction was concomitant with a marked increase in both the number of bonds formed and those broken. When the number of bonds formed and broken reached a steady-state value the average friction was lower than it was at the start of the simulation.

Donnet and Grill have shown that under ultrahigh vacuum conditions friction in DLC films is strongly affected by the hydrogen content of the films.[43] Hydrogen content lower than 34% systematically led to high friction. Ultralow friction was achieved with films that contained at lease 40% hydrogen. Our results clearly indicate that unsaturated carbon atoms in the film (sp^2 carbon) can undergo chemical reactions that lead to adhesion between the counterface and the film, increasing the friction. We can infer that adding hydrogen atoms to the film saturates the sp^2 carbon, may reduce the adhesive contribution to the friction.

We should also point out that the thickness of the amorphous films had no influence on the calculated friction. Thus, it seems clear that the structure of the film near the interface is what is dominating the friction. Indeed, the structure of the surfaces of the thick- and thin-film systems examined here were nearly identical.

Acknowledgment. This work was supported by the U.S. Office of Naval Research and by The Air Force Office of Scientific Research under contracts N00014-02-WR-20180 and NMIPR-02-5203507, respectively. The authors also thank Dr. S. Zybin for valuable discussions.

JA0178618

(42) Carpick, R. W. Private communication.

(43) Donnett, C.; Grill, A. *Surf. Coat. Technol.* **1997**, *94*−*95*, 456−462.